Supplementary Information: Depolarization dynamics in a strongly interacting solid state spin ensemble

Joonhee Choi,* Soonwon Choi,* Georg Kucsko,* Peter C. Maurer, Brendan J. Shields, Hitoshi Sumiya, Shinobu Onoda, Junichi Isoya, Eugene Demler, Fedor Jelezko, Norman Y. Yao, and Mikhail D. Lukin

(Dated: January 31, 2017)

CONTENTS

FLUORESCENCE DYNAMICS

We utilize a green laser (λ = 532 nm) to initialize and read out the spin state of NV centers. Due to a two-photon absorption process this excitation can cause ionization of NV centers, resulting in an out-of-equilibrium charge distribution around the excitation spot. This charge distribution relaxes even without illumination, as discussed in the main text. In practice, such charge dynamics can affect the spin-state readout by changing the average fluorescence emission rates (NV^0 vs NV^-). In this section, we explain how to avoid this problem.

The effect of charge dynamics on fluorescence emission rate is illustrated in Fig. S1a. Under green laser illumination (0 - 200 μs) the fluorescence emission rate initially increases as spins are polarized, but then quickly decreases as NV centers get ionized (due to preferential collection from the NV^- phonon sideband). Following the polarization of spins at varying laser power, we record the florescence after a variable time evolution t with and without an extra microwave π-pulse at the end of the evolution (empty and full circles Fig. S1a). We find that the observed fluorescence levels are asymmetric and for high power increase as a function of time. This fluorescence increase is caused by previously ionized NV centers, relaxing back to equilibrium. This effect is particularly dominant at high green excitation power, where ionization at the focal spot is increased. However, as demonstrated in Fig S1b, the difference in fluorescence with and without the extra π-pulse is independent from the applied green laser power. This result implies that one can use such a differential readout to mediate the contribution of charge dynamics and reliably extract the spin depolarization time scales. Additionally, the use of a low power green laser ($\sim$10 μW) can help reduce the effects of charge dynamics during the experiment. Note, that a similar technique has previously been used to robustly measure spin dynamics in high density NV samples [1].

ESTIMATION OF DIPOLAR SPIN DIFFUSION TIMESCALE

One potential mechanism of spin-density dependent depolarization is that polarized spins diffuse out of the probing volume via dipolar interactions. Here, we estimate the timescale of such spin diffusion using a classical diffusion equation. In our experiments, the probing volume is determined by the confocal excitation spot size $w \sim 200$ nm.

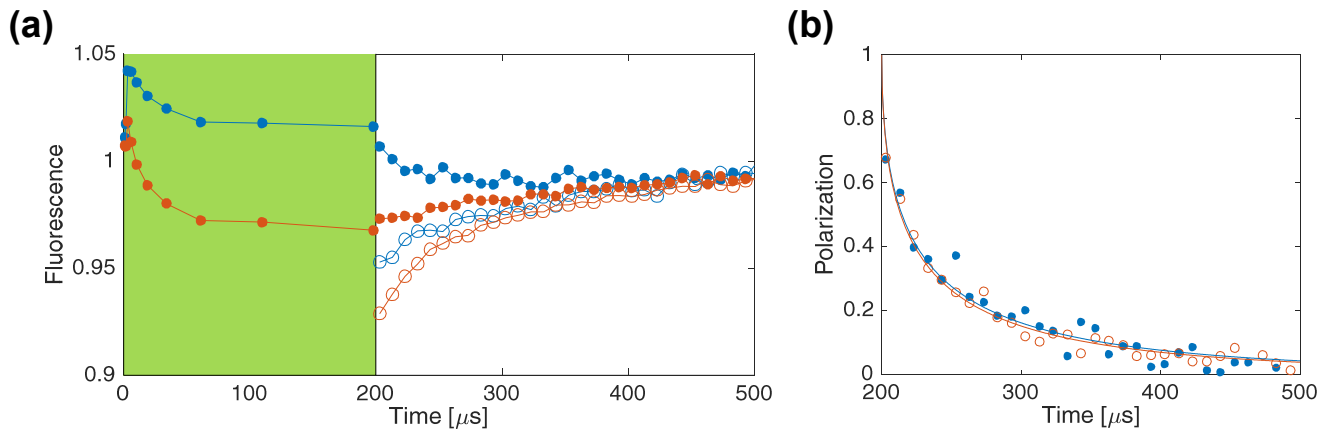

FIG. S1. **Fluorescence Dynamics. (a)** Fluorescence emission measurements for two different green laser powers, 10 μW (solid blue data) 40 μW (solid red data). An initial green laser pulse with length 200 μs is used to polarize the spin states of NV centers and reach a charge equilibrium state. After a wait time t, another green pulse is used to read out the spin state. The fluorescence emission rate is measured for both the polarization pulse (green background) and the readout pulse (white background, as a function of t). The emission rate is normalized by an equilibrium value obtained at sufficiently late time (> 500 μs). Empty circles correspond to similar measurements with the addition of microwave π-pulse shortly before readout. **(b)** Spin polarization decay as a function of time, extracted from the difference between filled and empty circles from (a) for both excitation powers.

Note that this estimate assumes a bulk diamond excitation, approximated by a 2D model, due to the large extent of the excitation spot in the direction normal to the diamond surface. The effective diffusion coefficient D can then be estimated from the average spacing among NV centers $a \sim 5$ nm and the typical flip-flop time $\tau \sim 9.5$ μs (calculated from $J/4 = (2\pi)$ 105 kHz), $D \approx a^2/\tau \sim 2.6$ nm$^2/\mu$s. Assuming that the spin polarization initially follows a Gaussian distribution with spatial width w, the classical diffusion equation predicts the polarization profile at later time t

$$P(t,\vec{r}) = \frac{e^{-\frac{r^2}{2(w^2+Dt)}}}{2(w^2+Dt)\pi}, \tag{S1}$$

where one finds that the spin polarization density at $r = 0$ is reduced by a factor of 2 at time $t \sim w^2/D \sim 15$ ms. This timescale is more than two orders of magnitude slower than experimentally measured depolarization times. We note that our estimation ignores the effect of inhomogeneous distribution of NV transition frequencies arising from the presence of other magnetic impurities in diamond; such disorder in transition energies further suppresses resonant spin flip-flop dynamics. For this reason, we rule out spin diffusion as the sole mechanism of ensemble depolarization.

RATE EQUATION MODEL: SPIN-STATE DEPENDENT DEPOLARIZATION

In order to estimate the decay rates of two independent depolarization channels γ_1 and γ_2 (Fig. 1a, main text), we analyze the population changes in $|m_s = 0\rangle$ and $|m_s = +1\rangle$ after initialization into $|m_s = -1\rangle$ (Fig. S2b). For this we employ the following simple rate equation model

$$\frac{d}{dt}\begin{bmatrix} P^{|-1\rangle} \\ P^{|0\rangle} \\ P^{|+1\rangle} \end{bmatrix} = \begin{bmatrix} -\gamma_1-\gamma_2 & \gamma_1 & \gamma_2 \\ \gamma_1 & -2\gamma_1 & \gamma_1 \\ \gamma_2 & \gamma_1 & -\gamma_1-\gamma_2 \end{bmatrix} \begin{bmatrix} P^{|-1\rangle} \\ P^{|0\rangle} \\ P^{|+1\rangle} \end{bmatrix},$$

where $P^{|-1\rangle}, P^{|0\rangle}$, and $P^{|+1\rangle}$ are the normalized populations in each spin states. When spins are initialized into $|m_s = -1\rangle$ at $t = 0$, the solution of the rate equation model predicts

$$P^{|-1\rangle}(t) - P^{|0\rangle}(t) = \frac{1}{2}e^{-(\gamma_1+2\gamma_2)t} + \frac{1}{2}e^{-3\gamma_1 t} \tag{S2}$$

$$P^{|0\rangle}(t) - P^{|+1\rangle}(t) = \frac{1}{2}e^{-(\gamma_1+2\gamma_2)t} - \frac{1}{2}e^{-3\gamma_1 t}. \tag{S3}$$

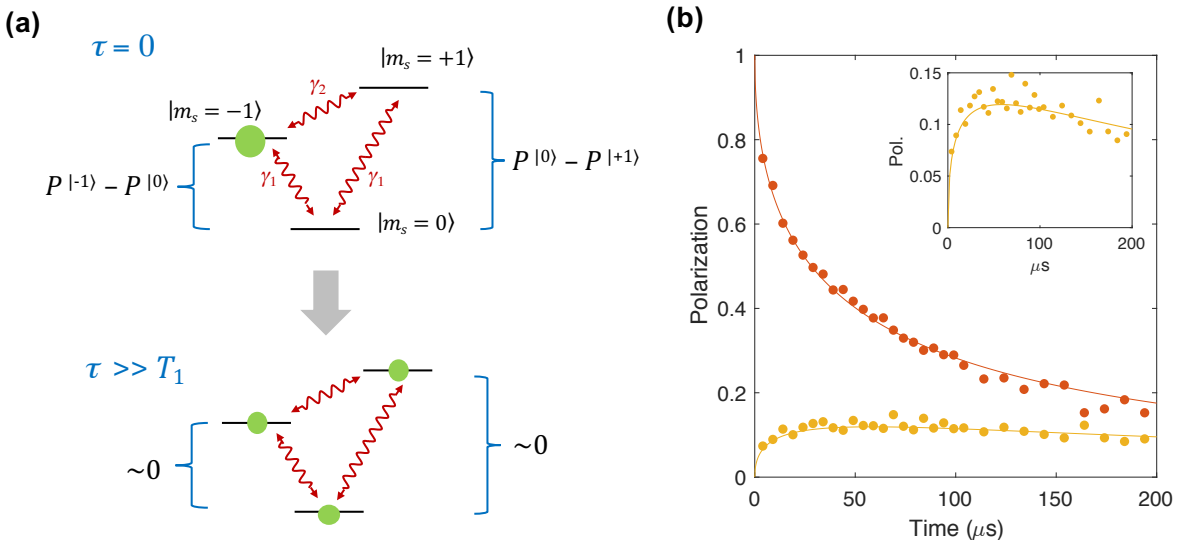

FIG. S2. **Magnetic Noise Model. (a)** Schematic level diagram depicting population distribution at $\tau = 0$ (after initialization into $|-1\rangle$) and at $\tau >> T_1$. Possible relaxation channels with rates γ_1 and γ_2 are indicated as red arrows. **(b)** Population difference over time between $|-1\rangle$ and $|0\rangle$ (red data) as well as between $|+1\rangle$ and $|0\rangle$ (orange data) after initialization into $|-1\rangle$. Solid lines indicate the results of the rate equation model, fit to the data. Inset shows a zoom-in of the $|+1\rangle$ - $|0\rangle$ data for better visibility.

In our experiments, however, the decay rates γ_1 and γ_2 are random variables, giving rise to stretched exponential profiles. Consequently, the measured population differences become

$$P^{|-1\rangle}(t) - P^{|0\rangle}(t) = \frac{1}{2}e^{-\sqrt{(\gamma_1+2\gamma_2)t}} + \frac{1}{2}e^{-\sqrt{3\gamma_1 t}} \tag{S4}$$

$$P^{|0\rangle}(t) - P^{|+1\rangle}(t) = \frac{1}{2}e^{-\sqrt{(\gamma_1+2\gamma_2)t}} - \frac{1}{2}e^{-\sqrt{3\gamma_1 t}}. \tag{S5}$$

Fitting Eq. (S4) and (S5) to experimental data, we extract $\gamma_1 = 10.6 \pm 0.6$ kHz and $\gamma_2 = 1.1 \pm 0.7$ kHz. As shown in Fig. S2b, this simple theory prediction and the experiment data are in excellent agreement. In particular, we notice that $\gamma_1 \gg \gamma_2$, implying that the spin state decay is induced by a local magnetic noise which changes only one unit of magnetization at a time, $\Delta m_s = \pm 1$.

DETAILED ANALYSIS OF SPIN-FLUCTUATOR MODEL

In this section, we provide a detailed analysis of our fluctuator model. As described in the main text, we assume that a fraction of NV centers, with density n_f, undergo rapid depolarization at rate γ_f. Their positions and orientations are randomly distributed. These fluctuators interact with normal spins via dipolar interactions, inducing depolarization. Here, we derive four characteristic features of the observed depolarization dynamics presented in the main text: (a) spin-state dependent polarization rates and preferential decay, (b) stretched exponential decay of ensemble polarization, (c) the resonant feature of depolarization rates as two groups of NV centers become degenerate, and (d) the extension of spin lifetime via spin-locking. Note that the quantitative analysis in (c) allows us to extract the values of γ_f and n_f from the experimental data presented in the main text (Fig. 2c main text). We use those extracted parameters to predict the spin lifetime T_1^ρ under spin-locking, which shows reasonable agreement with the data (Fig. 2d main text).

This section is organized in the following order. First, we compute the effective depolarization rate of a normal spin induced by dipolar interaction with a single fluctuator. We will show that such a mechanism results in spin-state dependent T_1 and preferential decay. Second, we show that interactions with multiple fluctuators located at random positions results in a distribution of effective decay rates $\rho(\gamma)$. We will explicitly compute the ensemble depolarization $P(t) = \int_0^\infty \rho(\gamma) e^{-\gamma t} d\gamma = e^{-\sqrt{t/T_1}}$ and provide an analytic expression for T_1 in terms of microscopic parameters. Finally, we will apply these results to various scenarios to predict the resonant features in Fig. 2c of the main text and the extension of spin lifetime in Fig. 2d of the main text.

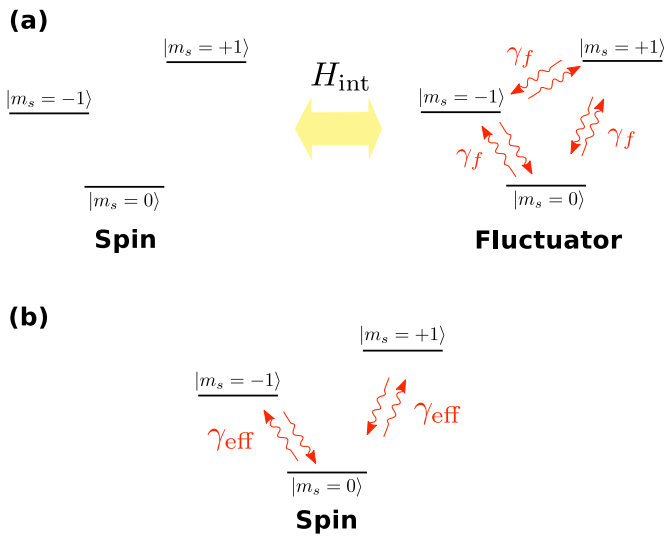

FIG. S3. **Spin-Fluctuator interaction (a)** Level diagram showing a single spin interacting with a single fluctuator. The fluctuator undergoes rapid incoherent depolarization at a rate γ_f. **(b)** Effective incoherent dynamics of a spin due to fluctuator interactions.

Single Spin Interacting with a Single Fluctuator

We begin our analysis by considering a system of a single spin and a single fluctuator that interact via Hamiltonian H_{int}. The total Hamiltonian of such a system is given as

$$H = H_1 + H_2 + H_{\text{int}} \tag{S6}$$

where H_1 and H_2 are single particle Hamiltonians for a normal spin and a fluctuator, respectively. The details of H_1 and H_2 varies over different experiments. For example, in typical T_1 measurements where an external magnetic field is aligned along the quantization axis of NV centers, the single particle Hamiltonians are diagonal in the natural spin basis $H_{1/2} = \sum_{m_s\in\{0,\pm1\}} \omega_{m_s} |m_s\rangle \langle m_s|$, where the energy eigenvalues ω_{m_s} in the rotating frame are random number of order $W \sim (2\pi)$ 9 MHz, owing to inhomogeneous broadening of the system. When strong spin-locking with Rabi frequency Ω is applied between $|m_s=0\rangle$ and $|m_s=-1\rangle$ transition, a dressed state basis is preferred, where $H_{1/2} = \pm(\Omega/2)|\pm\rangle\langle\pm| + \omega_0 |m_s=0\rangle\langle m_s=0|$ with $|\pm\rangle = (|m_s=0\rangle \pm |m_s=-1\rangle)/\sqrt{2}$ as defined in the main text. Later, we will also consider a situation where H_1 and H_2 are diagonal in the different basis. Such a case arises when the normal spin and the fluctuator are oriented in different directions. Here, for simplicity, we assume a generic eigenbasis $\{|i\rangle\}$ and $\{|\alpha\rangle\}$ for H_1 and H_2, so that

$$H_1 = \sum_{i\in\{1,2,3\}} \omega_i |i\rangle\langle i| \quad \text{and} \quad H_2 = \sum_{\alpha\in\{a,b,c\}} \omega_\alpha |\alpha\rangle\langle\alpha|\,, \tag{S7}$$

where ω_i and ω_α are corresponding energies in the rotating frame. In addition to coherent dynamics, the fluctuator undergoes rapid incoherent dynamics. Hence, the dynamics of the system are governed by a quantum master equation

$$\dot{\rho} = -i[H,\rho] + L[\rho] \tag{S8}$$

$$L[\rho] = \sum_k L_k \rho L_k^\dagger - \frac{1}{2}\left(L_k^\dagger L_k \rho + \rho L_k^\dagger L_k\right), \tag{S9}$$

where ρ is the density matrix of the system and L_k are decay operators. In our model, we consider six decay processes as illustrated in Fig. S3(a) with identical decay rates γ_f, i.e., $L_k = \sqrt{\gamma_f}\,|m_s=\alpha\rangle\langle m_s=\beta|$ with $(\alpha,\beta) \in \{(+1,-1),(-1,+1),(+1,0),(0,+1),(-1,0),(0,-1)\}$.

In order to derive the effective master equation for a spin, we use the Born-Markov approximation together with secular approximations [2]. In such a description, the quantum state of the system is approximated by $\rho = \rho_1 \otimes \rho_{\text{thm}}$, where ρ_1 is the reduced density matrix of the normal spin and ρ_{thm} is the equilibrium state of the fluctuator, such that

$L[\rho_1 \otimes \rho_{\rm rhm}] = 0$. In our model, the equilibrium state is a maximally mixed state $\rho_{\rm thm} = \frac{1}{3}I$. These approximations are well justified due to the hierarchy of the coupling strengths $J_{ij} \ll |\omega_{ij}| \ll \gamma_f$, where $\omega_{ij} = \omega_i - \omega_j$ are the energy difference between eigenstates and J_{ij} are typical dipolar interaction strengths. Under these approximations, the effective dynamics of a spin become

$$\dot{\rho_1} = -i[H_1, \rho_1] + L^{\rm eff}[\rho_1], \tag{S10}$$

where the first and second terms describe the coherent dynamics by the Hamiltonian H_1 and the induced dynamics by interactions with the fluctuator, respectively. Following standard procedures [2], we obtain

$$L^{\rm eff}[\rho] \approx \sum_{i,j} \sum_{\alpha\beta\gamma\delta} C^{ij}_{\alpha\beta} C^{ji}_{\gamma\delta} S^{\alpha\beta\gamma\delta}(\omega_{ij}) \Big[|j\rangle\langle i| \, \rho \, |i\rangle\langle j| - |i\rangle\langle i| \, \rho \Big] + h.c. \tag{S11}$$

$$+ \sum_{i\neq k} \sum_{\alpha\beta\gamma\delta} C^{ii}_{\alpha\beta} C^{kk}_{\gamma\delta} S^{\alpha\beta\gamma\delta}(\omega_{ij}) \Big[|k\rangle\langle k| \, \rho \, |i\rangle\langle i| - |i\rangle\langle i| \, |k\rangle\langle k| \, \rho \Big] + h.c. \tag{S12}$$

where $C^{ij}_{\alpha\beta}$ is a matrix element of the interaction defined as $C^{ij}_{\alpha\beta} \equiv \langle i\alpha| \, H_{\rm int} \, |j\beta\rangle$ with $i, j \in \{1, 2, 3\}$ and $\alpha, \beta \in \{a, b, c\}$, and $S^{\alpha\beta\gamma\delta}$ is the spectral response function of the fluctuator defined as

$$S^{\alpha\beta\gamma\delta}(\omega) = \int_0^\infty e^{i\omega\tau} \, \langle\beta| \, e^{\tau\mathcal{L}_2} \Big[|\gamma\rangle \, \langle\delta| \, \rho_{\rm thm} \Big] \, |\alpha\rangle \, . \tag{S13}$$

where the superoperator $\mathcal{L}_2[\cdot] = -i[H_2, \cdot] + L[\cdot]$ describes the time evolution of the fluctuator. For the decay channels illustrated in Fig. S3, the spectral response function $S^{\alpha\beta\gamma\delta}$ can be simplified by

$$S^{\alpha\beta\gamma\delta}(\omega) = \delta_{\beta\gamma}\delta_{\alpha\delta} S^{\alpha\beta}(\omega) \equiv \delta_{\beta\gamma}\delta_{\alpha\delta} \begin{cases} \frac{1}{3} \cdot \frac{1}{i(\omega+\omega_{\alpha\beta})-2\gamma_f} & \text{for } \alpha \neq \beta \\ \frac{1}{9} \cdot \left(\frac{1}{i\omega} + \frac{2}{i\omega-3\gamma_f} \right) & \text{for } \alpha = \beta \end{cases} . \tag{S14}$$

Since $H_{\rm int}$ is Hermitian, we can use the relation $C^{ij}_{\alpha\beta} = (C^{ji}_{\beta\alpha})^*$ to obtain

$$L^{\rm eff}[\rho] \approx \sum_{i,j} \sum_{\alpha\beta} |C^{ij}_{\alpha\beta}|^2 S^{\alpha\beta}(\omega_{ij}) \Big[|j\rangle\langle i| \, \rho \, |i\rangle\langle j| - |i\rangle\langle i| \, \rho \Big] + h.c. \tag{S15}$$

$$+ \sum_{i\neq k} \sum_{\alpha\beta} C^{ii}_{\alpha\beta} C^{kk}_{\beta\alpha} S^{\alpha\beta}(0) \Big[|k\rangle\langle k| \, \rho \, |i\rangle\langle i| - |i\rangle\langle i| \, |k\rangle\langle k| \, \rho \Big] + h.c. \tag{S16}$$

Finally, introducing

$$\Gamma_{ij} = 2 \sum_{\alpha\beta} |C^{ij}_{\alpha\beta}|^2 {\rm Re}\Big[S^{\alpha\beta}(\omega_{ij}) \Big] \quad \& \quad \Delta_{ij} = 2 \sum_{\alpha\beta} |C^{ij}_{\alpha\beta}|^2 {\rm Im}\Big[S^{\alpha\beta}(\omega_{ij}) \Big], \tag{S17}$$

the effective superoperator simply becomes

$$L^{\rm eff}[\rho] = \sum_{ij} \Gamma_{ij} \Big[|j\rangle\langle i| \, \rho \, |i\rangle\langle j| - \frac{1}{2} \left(|i\rangle\langle i| \, \rho + \rho \, |j\rangle\langle j| \right) \Big] \tag{S18}$$

$$- i \sum_{ij} \Delta_{ij} \big[\, |i\rangle\langle i| \, , \rho \big] \tag{S19}$$

$$+ \sum_{i\neq k} \sum_{\alpha\beta} C^{ii}_{\alpha\beta} C^{kk}_{\beta\alpha} S^{\alpha\beta}(0) \Big[\, |k\rangle\langle k| \, \rho \, |i\rangle\langle i| \, \Big] + h.c. \tag{S20}$$

Here, we clearly see three types of terms: (i) depolarization or dephasing at rates Γ_{ij}, (ii) energy corrections Δ_{ij} to coherent dynamics, and (iii) additional dephasing from diagonal interactions. Here, we are most interested in the depolarization processes Γ_{ij} under various conditions. In particular, we note that the dipolar interaction under secular approximation is given by

$$H_{\rm int} \approx -J_0/r^3 \big[\, (g + ih) \, (|+1, 0\rangle\langle 0, +1| + |0, -1\rangle\langle -1, 0|) + h.c. + q S^z_i S^z_j \big], \tag{S21}$$

where $J_0 = (2\pi)\ 52\ \text{MHz}\cdot\text{nm}^3$ is the dipolar interaction strength, r is the distance, and g, h, and q are coefficients of order unity that depend on the relative orientation of the spin and fluctuator:

$$g = \frac{1}{2}\Big[3\,(\hat{r}\cdot\hat{x}_s)\,(\hat{r}\cdot\hat{x}_f) - \hat{x}_s\cdot\hat{x}_f + 3\,(\hat{r}\cdot\hat{y}_s)\,(\hat{r}\cdot\hat{y}_f) - \hat{y}_s\cdot\hat{y}_f\Big] \tag{S22}$$

$$h = \frac{1}{2}\Big[3\,(\hat{r}\cdot\hat{x}_s)\,(\hat{r}\cdot\hat{y}_f) - \hat{x}_s\cdot\hat{y}_f - 3\,(\hat{r}\cdot\hat{y}_s)\,(\hat{r}\cdot\hat{x}_f) + \hat{y}_s\cdot\hat{x}_f\Big] \tag{S23}$$

$$q = 3\,(\hat{r}\cdot\hat{z}_s)\,(\hat{r}\cdot\hat{z}_f) - \hat{z}_s\cdot\hat{z}_f \tag{S24}$$

with unit vectors $(\hat{x}_a, \hat{y}_a, \hat{z}_a)$ characterizing the quantization axis of the spin ($a = s$) or fluctuator ($a = f$) [3]. If the quantization axes of the spin and fluctuator coincide, we get the simplified expressions for $g = (1 - 3\cos^2\theta)/2, h = 0$, and $q = -(1 - 3\cos^2\theta)$ with $\cos\theta \equiv \hat{z}_{s,f}\cdot\hat{r}$. Importantly, as seen in the Eq. (S21), the interaction does not contain any transitions between $|m_s = +1\rangle$ to $|m_s = -1\rangle$, resulting in vanishing decay rates between the two states, i.e. $\Gamma_{+1,-1} = \Gamma_{-1,+1} = 0$. Consequently, the interaction-induced dynamics of a spin can be modeled as in Fig. S3, which exhibit spin-state dependent depolarization rates as well as preferential decays described in the previous section. More specifically, the induced decay rate is

$$\gamma_s(\vec{r}) = \left(\frac{J_0}{r^3}\right)^2 \frac{\eta^2}{\gamma_f}, \tag{S25}$$

where $\delta\omega$ and r are the energy difference (due to inhomogeneous broadening) and distance between the spin and the fluctuator, respectively, and η is a dimensionless number of order unity that characterizes the orientation dependent coefficients of the dipolar interaction as well as spectral responses

$$\eta^2 \equiv \frac{2}{3}(|g|^2 + |h|^2)\frac{2\gamma_f^2}{(\delta\omega)^2 + 4\gamma_f^2}. \tag{S26}$$

Derivation of the Stretched Exponential Decay

In an ensemble, the net decay rate γ_s^{eff} of a spin is given as the sum of rates induced by multiple nearby fluctuators, $\gamma_s^{\text{eff}} = \sum_i \gamma_s(\vec{r}_i)$, where $\gamma_s(\vec{r}_i)$ is the decay rate induced by fluctuator i located at position $\vec{r}_i$ (see Eq. (S25)). Consequently, the decay rates vary from one spin to another, and the ensemble polarization decays as sum of multiple simple exponentials, whose temporal profile depends on the probability distribution of effective decay rates $\rho(\gamma)$. Here, we compute this distribution and show that the ensemble polarization decays as a stretched exponential

$$P(t) = e^{-\sqrt{t/T_1}}. \tag{S27}$$

We will see that the exponent, 1/2, arises as a consequence of incoherent dipole-dipole interaction in 3D. We start with a single spin located at the origin $\vec{r} = 0$ and consider its effective depolarization rate induced by fluctuators at $\{\vec{r}_1, \vec{r}_2, \ldots, \vec{r}_N\}$ The polarization decays as a simple exponential with the rate given by $\gamma_s^{\text{eff}} = \sum_i \gamma_s(\vec{r}_i)$. From the previous section (Eq. (S25)), we have shown that each $\gamma_i \equiv \gamma_s(\vec{r}_i)$ can be written as $\gamma_i = \frac{J_0^2}{r_i^6}\frac{\eta_i^2}{\gamma_f}$. The probability distribution $\rho(\gamma_s^{\text{eff}})$ is obtained by averaging $\delta\left(\sum_i \gamma_i - \gamma_s^{\text{eff}}\right)$ over all possible configurations of fluctuators: different number N, positions, and orientations

$$\rho(\gamma_s^{\text{eff}}) = \int d\{\vec{r}_i\}\ \text{Prob}(\{\vec{r}_i\})\ \delta\left(\sum_i \gamma_i - \gamma_s^{\text{eff}}\right). \tag{S28}$$

When the positions of fluctuators are homogeneously distributed with density n_f, we can analytically compute $\rho(\gamma_s^{\text{eff}})$:

$$\rho(\gamma_s^{\text{eff}}) = \sum_N \int_{\mathcal{D}} dr_1 \ldots dr_N \left(\prod_{i=1}^{N} e^{-\frac{4\pi}{3}n_f(r_i^3 - r_{i-1}^3)} 4\pi n_f r_i^2\right) e^{-\frac{4\pi}{3}n_f(R^3 - r_N^3)} \left\langle \delta\left(\sum_i \gamma_i - \gamma_s^{\text{eff}}\right)\right\rangle_\eta \tag{S29}$$

$$= \int_{-\infty}^{\infty} dz \frac{e^{i\gamma_s^{\text{eff}} z}}{\sqrt{2\pi}} \sum_N \int_{\mathcal{D}} dr_1 \ldots dr_N \left(\prod_{i=1}^{N} e^{-\frac{4\pi}{3}n_f(r_i^3 - r_{i-1}^3)} 4\pi n_f r_i^2 \left\langle e^{-i\gamma_i z}\right\rangle_\eta\right) e^{-\frac{4\pi}{3}n_f(R^3 - r_N^3)} \tag{S30}$$

where the domain of the integral is $\mathcal{D} = r_0 \le r_1 \le r_2 \cdots \le r_N \le R$ with the shortest (largest) distance cut-off r_0 (R), z is a dummy variable introduced for $\delta(x) = \int_{-\infty}^{\infty} dz e^{ixz}/\sqrt{2\pi}$, and $\langle\cdot\rangle_\eta$ represents the averaging of all possible orientations of a fluctuator with fixed distance. We denote this distribution with Prob(η). Now, we see that

$$\rho(\gamma_s^{\rm eff}) = \int_{-\infty}^{\infty} dz \frac{e^{i\gamma_s^{\rm eff} z}}{\sqrt{2\pi}} e^{-\frac{4\pi}{3} n_f (R^3 - r_0^3)} \sum_N \frac{1}{N!} \left[\int_{r_0}^{R} 4\pi n_f r^2 dr \int \mathrm{Prob}(\eta)\, d\eta\, e^{-i\frac{J_0^2}{\gamma_f r_i^6}\eta^2 z} \right]^N \tag{S31}$$

$$= \int_{-\infty}^{\infty} dz \frac{e^{i\gamma_s^{\rm eff} z}}{\sqrt{2\pi}} e^{-\frac{4\pi}{3} n_f (R^3 - r_0^3)} \sum_N \frac{1}{N!} \left[\int_{u_0}^{U} \frac{4\pi n_f}{3} du \int \mathrm{Prob}(\eta)\, d\eta \sqrt{(J_0^2\eta^2/\gamma_f)|z|} e^{-i\frac{\mathrm{sgn}(z)}{u^2}} \right]^N \tag{S32}$$

where we introduced $u = r^3/\sqrt{(J_0^2\eta^2/\gamma_f)|z|}$ and similarly u_0 and U for $r = r_0$ and $r = R$. Here, the integration over u can be done analytically. Note that we are interested in the limit of large R and small r_0, which corresponds to $u_0 \ll 1$ (behavior at long enough time) and $U \gg 1$ (before the boundary effect becomes relevant).

$$\int_{u_0}^{U} du e^{-i\,\mathrm{sgn}(z)/u^2} \approx U - (1 + \mathrm{sgn}(z)i)\sqrt{\pi/2}. \tag{S33}$$

Finally, we obtain

$$\rho(\gamma) \approx \int_{-\infty}^{\infty} dz \frac{e^{i\gamma z}}{\sqrt{2\pi}} e^{-\frac{4\pi n_f}{3}\sqrt{\pi/2}(1+\mathrm{sgn}(z)i)\int \mathrm{Prob}(\eta)\sqrt{(J_0^2\eta^2/\gamma_f)|z|}d\eta} \tag{S34}$$

$$= \int_{-\infty}^{\infty} dz \frac{e^{i\gamma z}}{\sqrt{2\pi}} e^{(iz/T)^{1/2}} = \frac{e^{-1/(4\gamma T)}}{\sqrt{4\pi\gamma^3 T}} \tag{S35}$$

where we introduced the time scale

$$\frac{1}{T} \equiv \left(\frac{4\pi n_f J_0 \bar{\eta}}{3}\right)^2 \frac{\pi}{\gamma_f} \tag{S36}$$

with the orientation averaged $\bar{\eta} \equiv \int \mathrm{Prob}(\eta)\ \eta\ d\eta$. The ensemble depolarization profile $P(t)$ can be computed from $\rho(\gamma_s^{\rm eff})$:

$$P(t) = \int_0^{\infty} \rho(\gamma) e^{-\gamma t} d\gamma = e^{-\sqrt{t/T}}. \tag{S37}$$

Dependence of depolarization dynamics on dimensionality and interaction strengths

More generally, we derive the functional form of $P(t)$ for a d-dimensional spin ensemble with different interaction strengths. We assume that the interaction between a spin and a fluctuator scales as $1/r^\alpha$, where $\alpha > d/2$. Generalizing Eq. (S29) for d-dimensional systems, we rewrite the probability distribution of the induced spin decay rate as

$$\rho(\gamma_s^{\rm eff}) = \sum_{N=0}^{\infty} \int_{\mathcal{D}} \left(\prod_{i=1}^{N} dr_i\ e^{-\frac{n_f A_d}{d}(r_i^d - r_{i-1}^d)} n_f A_d r_i^{d-1} \right) e^{-\frac{n_f A_d}{d}(R^d - r_N^d)} \left\langle \delta\left(\sum_i \gamma_i - \gamma_s^{\rm eff} \right) \right\rangle_\eta , \tag{S38}$$

where $A_d = 2\pi^{d/2}/\Gamma(d/2)$ is the surface area of a d-dimensional sphere of unit radius. The ensemble depolarization in d-dimension can be expressed as:

$$P(t) = \int_0^\infty \rho(\gamma_s^{\text{eff}}) e^{-\gamma_s^{\text{eff}} t} d\gamma_s^{\text{eff}} \tag{S39}$$

$$= \sum_{N=0}^{\infty} \int_{\mathcal{D}} \left(\prod_{i=1}^{N} dr_i \; n_f A_d r_i^{d-1} \right) e^{-\frac{n_f A_d}{d}(R^d - r_0^d)} e^{-\sum_i \gamma_i t} \tag{S40}$$

$$= \sum_{N=0}^{\infty} \int_{\mathcal{D}} \left(\prod_{i=1}^{N} dr_i \; n_f A_d r_i^{d-1} e^{-\gamma_i t} \right) e^{-\frac{n_f A_d}{d}(R^d - r_0^d)} \tag{S41}$$

$$= \sum_{N=0}^{\infty} \int_{\mathcal{D}} \left(\prod_{i=1}^{N} dr_i \; n_f A_d r_i^{d-1} \exp\left\{ -\left(\frac{J_0}{r_i^\alpha}\right)^2 \frac{\eta_i^2}{\gamma_f} t \right\} \right) e^{-\frac{n_f A_d}{d}(R^d - r_0^d)} \tag{S42}$$

$$= \sum_{N=0}^{\infty} \frac{1}{N!} \left[\int_{r_0}^{R} dr \; n_f A_d r^{d-1} \exp\left\{ -\left(\frac{J_0}{r^\alpha}\right)^2 \frac{\bar{\eta}^2}{\gamma_f} t \right\} \right]^N e^{-\frac{n_f A_d}{d}(R^d - r_0^d)} \tag{S43}$$

$$= \exp\left[\int_{r_0}^{R} dr \; n_f A_d r^{d-1} \exp\left\{ -\left(\frac{J_0}{r^\alpha}\right)^2 \frac{\bar{\eta}^2}{\gamma_f} t \right\} \right] e^{-\frac{n_f A_d}{d}(R^d - r_0^d)} \tag{S44}$$

Here we used $\gamma_i = \left(\frac{J_0}{r_i^\alpha}\right)^2 \frac{\eta_i^2}{\gamma_f}$, and $r_0(R)$ is the shortest (largest) cut-off distance. Changing the integration variable r to $z = (J_0^2 \bar{\eta}^2 t/\gamma_f)^{-\frac{d}{2\alpha}} r^d$, we simplify the above expression,

$$P(t) = \exp\left[\frac{n_f A_d}{d} \left(\frac{J_0^2 \bar{\eta}^2 t}{\gamma_f} \right)^{\frac{d}{2\alpha}} \int_{z_0}^{Z} dz \; \exp(-z^{-2\alpha/d}) \right] e^{-\frac{n_f A_d}{d}(R^d - r_0^d)}, \tag{S45}$$

where $z_0 = (J_0^2 \bar{\eta}^2 t/\gamma_f)^{-\frac{d}{2\alpha}} r_0^d$ and $Z = (J_0^2 \bar{\eta}^2 t/\gamma_f)^{-\frac{d}{2\alpha}} R^d$. We note that $\exp(-z^{-\frac{2\alpha}{d}})$ is a monotonically increasing function in z $\in (0, \infty)$ bounded by,

$$\lim_{z \to 0} \exp(-z^{-\frac{2\alpha}{d}}) = 0, \tag{S46}$$

$$\lim_{z \to \infty} \exp(-z^{-\frac{2\alpha}{d}}) = 1. \tag{S47}$$

Therefore, we find

$$\int_{z_0}^{Z} dz \; \exp(-z^{-\frac{2\alpha}{d}}) = (Z - z_0) - C, \tag{S48}$$

where $C = \int_{z_0}^{Z} dz \; [1 - \exp(-z^{-\frac{2\alpha}{d}})]$ is a non-zero positive constant. Substituting Eq. (S48) into Eq. (S45), we finally obtain

$$P(t) = \exp\left[\frac{n_f A_d}{d} \left(\frac{J_0^2 \bar{\eta}^2 t}{\gamma_f} \right)^{\frac{d}{2\alpha}} (Z - z_0 - C) \right] e^{-\frac{n_f A_d}{d}(R^d - r_0^d)} \tag{S49}$$

$$= \exp\left[-\frac{C n_f A_d}{d} \left(\frac{J_0^2 \bar{\eta}^2 t}{\gamma_f} \right)^{\frac{d}{2\alpha}} \right] \tag{S50}$$

$$= \exp\left[-(t/T_1)^{\frac{d}{2\alpha}} \right], \tag{S51}$$

where,

$$\frac{1}{T_1} = \left(\frac{C n_f A_d}{d} \right)^{\frac{2\alpha}{d}} \frac{J_0^2 \bar{\eta}^2}{\gamma_f}. \tag{S52}$$

As identified in Eq. (S51), the interplay between the dimensionality and the interaction strength determines the power of a stretched exponential decay. For three-dimensional dipolar-interacting spin ensembles ($\alpha = d = 3$), we recover the stretched exponential of power 1/2 ($= d/2\alpha$), being consistent with the experimental observations. For two-dimensional systems, a reduced power of 1/3 is expected if the spin-fluctuator exchange interaction is still a dominant source for spin depolarization.

Enhanced Depolarization of Two Degenerate Groups of NV Centers

When all four groups of NV centers with different quantization axes are spectrally separated, e.g. in Fig. 1b upper curve in the main text, the spin exchange interactions between NV centers in distinct groups are strongly suppressed due to a large energy mismatch. In such case, the depolarization dynamics of a spin are dominated by interactions with fluctuators within the same group. When two groups of NV centers are brought onto resonance, e.g. Fig. 1b lower curve in the main text, the inter-group dipolar interactions cannot be neglected, resulting in an enhanced effective depolarization rate. This effect can be quantitatively analyzed by modifying the probability distribution

$$\mathrm{Prob}(\eta) = \frac{1}{4}\,\mathrm{Prob}^{\mathrm{same}}(\eta) + \frac{1}{4}\,\mathrm{Prob}^{\mathrm{diff}}(\eta) + \frac{1}{2}\cdot 0, \tag{S53}$$

where $\mathrm{Prob}^{\mathrm{same}}(\eta)$ and $\mathrm{Prob}^{\mathrm{diff}}(\eta)$ correspond to the probability distributions of η for dipolar interactions within a group and between two near-resonant groups, respectively. The other two groups with probability $1/2$ do not induce resonant depolarization. Crucially, the latter distribution depends on the spectral distance δ because η is a function of energy mismatch between a spin and a fluctuator:

$$\eta^2 = \frac{2}{3}(|g|^2 + |h|^2)\frac{2\gamma_f^2}{(\delta\omega+\delta)^2 + 4\gamma_f^2}. \tag{S54}$$

Averaging over all orientations, we obtain

$$\int \mathrm{Prob}^{\mathrm{same}}(\eta)\;\eta\;d\eta = \sqrt{\frac{2}{3}}\cdot\frac{2}{3\sqrt{3}}\cdot\sqrt{\frac{2\gamma_f^2}{\delta\omega^2+4\gamma_f^2}} \tag{S55}$$

$$\int \mathrm{Prob}^{\mathrm{diff}}(\eta)\;\eta\;d\eta \simeq \sqrt{\frac{2}{3}}\times 0.6507\times\sqrt{\frac{2\gamma_f^2}{(\delta\omega+\delta)^2+4\gamma_f^2}}, \tag{S56}$$

where the middle factors arise from angular averaging of the matrix elements g and h of dipolar interactions. Interestingly, the angle-averaged matrix element of flip-flop interaction is slightly larger for inter-group interaction than for intra-group interaction $0.6507 > 2/3\sqrt{3}$, which explains the fact that the depolarization rate at the two-group resonance $\delta = 0$ is slightly larger than four times that of a single group. We note that for the theory curves presented in the main text we further average over the energy mismatch $\delta\omega$ arising from inhomogeneous broadening, which we model using a Gaussian distribution with full width at half maximum (FWHM) $W \sim (2\pi)\ 9$ MHz.

Extension of the Spin Lifetime via Spin-locking

Under strong driving conditions of a spin-locking sequence, the preferred quantization axes of spins and fluctuators are re-defined by the microwave driving. Specifically, in the rotating frame the eigenstates of a single particle Hamiltonian become $|\pm\rangle = (|m_s=0\rangle \pm |m_s=-1\rangle)/\sqrt{2}$ and $|m_s=+1\rangle$ with corresponding energy eigenvalues $\pm\Omega$ and 0 (up to on-site disorder due to the inhomogeneous broadening). Projecting the original, spin-1 Hamiltonian into the manifold of $|\pm\rangle$ states, we get the effective two-level Hamiltonian (in a rotating frame) for a driven spin ensemble with the same orientation,

$$H_{\mathrm{eff}} = H_0 + H_{dd}, \tag{S57}$$

where

$$H_0 = \sum_i (\Omega\sigma_i^x + \Delta_i\sigma_i^z) \tag{S58}$$

$$H_{dd} = \sum_{i,j}\frac{J_{ij}}{r_{ij}^3}\left[\sigma_i^x\sigma_j^x + \frac{1}{2}(\sigma_i^+\sigma_j^+ + \sigma_i^-\sigma_j^-)\right]. \tag{S59}$$

Here, $\sigma_i^x = |+\rangle_i\langle+| - |-\rangle_i\langle-|$, $\sigma_i^z = |+\rangle_i\langle-| + |-\rangle_i\langle+|$, $\sigma_i^\pm = |\pm\rangle_i\langle\mp|$, Δ_i is a random on-site disorder, r_{ij} is the distance between a NV center and a fluctuator, and J_{ij} is the orientation-dependent coefficient of the dipolar

interaction with typical strength $J_0 = (2\pi)\ 52\ \text{MHz}\cdot\text{nm}^3$. Interestingly, the flip-flop interactions in this $|\pm\rangle$ basis vanishes:

$$\langle +,-|\, H_{dd}\, |-,+\rangle = 0. \tag{S60}$$

This is in *stark* contrast to spin-1/2 systems in which H_{dd} contains non-vanishing exchange interactions, *i.e.,* $\langle +,-|\, H_{dd}\, |-,+\rangle = -J_0/r^3(g/2)$. In fact, the spin-1 nature of NV centers gives rise to such differences in the dipolar interaction of the effective Hamiltonian describing only two states. Therefore, as we prepare and lock spins along the $|\pm\rangle$ states by utilizing the spin-locking sequence, the depolarization time T_1^ρ can be significantly prolonged due to the absence of exchange interactions within these dressed-basis states. However, the enhanced spin lifetime T_1^ρ is still limited by other exchange processes between the driven $|\pm\rangle$ and undriven $|m_s = +1\rangle$ states. This additional spin exchange can be identified from the original interaction Hamiltonian H_{int} (see Eq. (S21)),

$$\langle \pm, m_s = +1|\, H_{\text{int}}\, |m_s = +1, \pm\rangle = -J_0/r^3(g/2). \tag{S61}$$

The matrix element of such a process is suppressed by a factor of 2, which, together with the three level nature of the rate model in Eq. (S2), leads to a factor of $2^2 \times 3 = 12$ improvement for T_1^ρ compared to T_1. For the theory curves presented in the main text (Fig. 4), we also include the effects of off-resonant interactions as well as interactions between different non-participant subensembles as in the previous section.

CHARGE DIFFUSION MODEL

To model the observed charge state dynamics, we consider a classical diffusion equation, $\partial_t \delta n = D(\partial_{xx} + \partial_{yy})\delta n$, where D is the diffusion constant and δn is the normalized excess or depletion of the NV^- charge state of NV centers compared to the equilibrium value (charge differential). We note that these charge diffusion experiments have been performed on a bulk piece of diamond under confocal excitation. However, due to the increased size of the confocal excitation spot in the direction normal to the diamond surface, we assume an effective 2D system. For a local electron tunneling process, the diffusion constant can be expressed as $D = a^2/T_{hop}$, where $a \sim 5$ nm is the typical NV separation, and T_{hop} is the electron hopping time. Figure S4a-d summarizes the prediction of the diffusion model for $T_{hop} = 10$ ns as a function of time, after the system is initialized into an out-of-equilibrium charge state (modeled after Fig. 4c main text). We calculate the expected rates of charge recovery at the center for various hopping rates, showing good agreement with the observed data when $T_{hop} \sim 10$ ns.

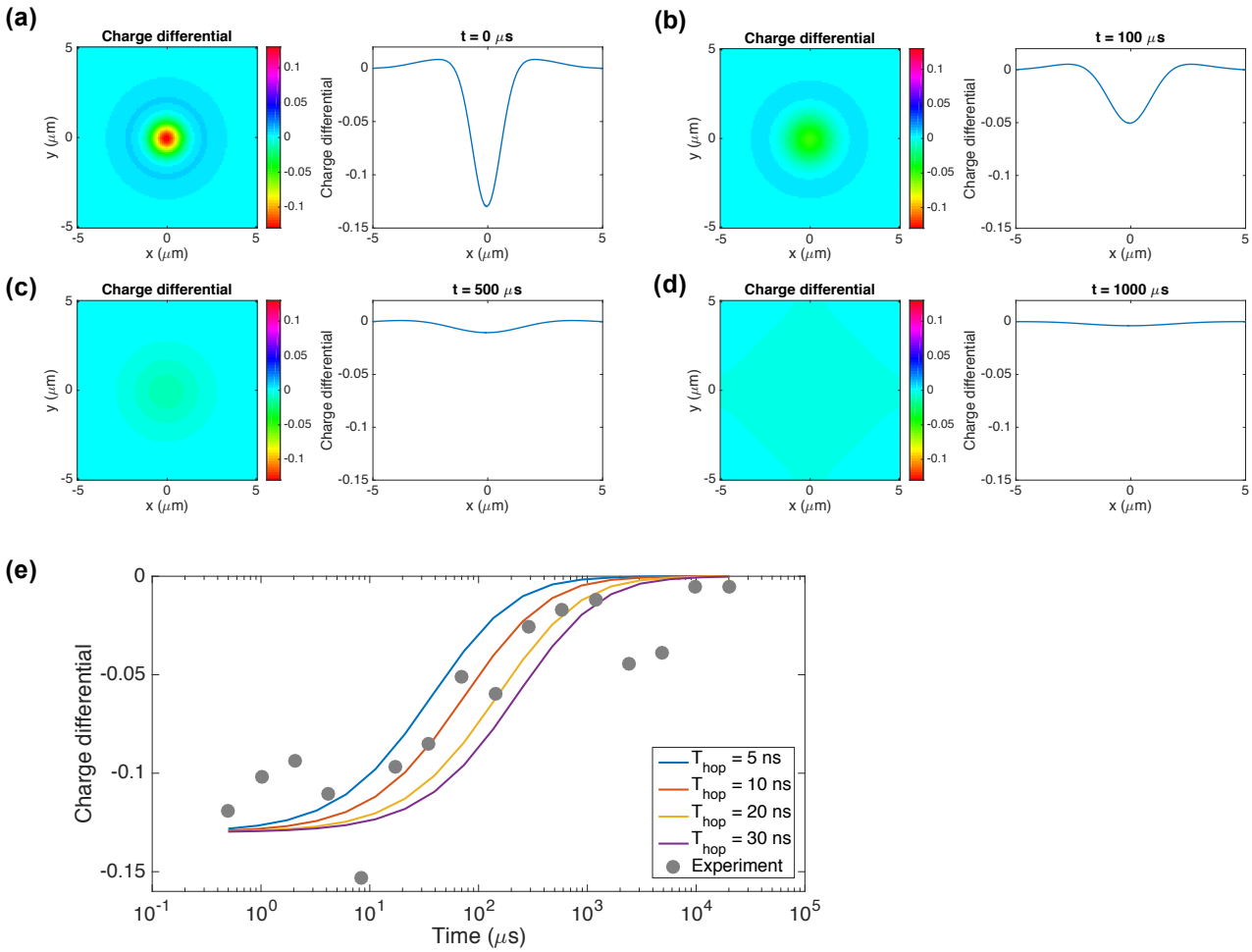

FIG. S4. **Charge-state Dynamics. (a)-(d)** Simulated two-dimensional charge distribution (relative increase of NV^- population compared to equilibrium) at different times after initialization, (a) $\tau = 0$, (b) $\tau = 100$, (c) $\tau = 500$ and (d) $\tau = 1000$ μs. We assumed an electron hopping timescale, $T_{hop} = 10$ ns, and typical hopping distance, $a = 5$ nm. **(e)** Charge differential at the center measured over time (grey data). Colored solid lines indicate the diffusion simulation results calculated for different hopping times T_{hop}.

---

* These authors contributed equally to this work

[1] M. Mrózek, D. Rudnicki, P. Kehayias, A. Jarmola, D. Budker, and W. Gawlik, EPJ Quantum Technology **2**, 1 (2015).
[2] C. Gardiner and P. Zoller, *Quantum noise: a handbook of Markovian and non-Markovian quantum stochastic methods with applications to quantum optics*, Vol. 56 (Springer Science & Business Media, 2004).
[3] G. Kucsko, S. Choi, J. Choi, P. C. Maurer, H. Sumiya, S. Onoda, J. Isoya, F. Jelezko, E. Demler, N. Y. Yao, and M. D. Lukin, arXiv preprint arXiv:1609.08216 (2016).